



## **Final Draft of the original manuscript**

Skoulas, D.; Mangiapia, G.; Parisi, D.; Kasimatis, M.; Glynos, E.;  
Stratikos, E.; Vlassopoulos, D.; Frielinghaus, H.; Iatrou, H.:

**Tunable Hydrogels with Improved Viscoelastic Properties from  
Hybrid Polypeptides.**

In: *Macromolecules*. Vol. 54 (2021) 23, 10786 – 10800.

First published online by ACS: 15.11.2021

<https://dx.doi.org/10.1021/acs.macromol.1c01596>

# Tunable Hydrogels with Improved Viscoelastic Properties from Hybrid Polypeptides.

Dimitrios Skoulas, Gaetano Mangiapia, Daniele Parisi, Maria Kasimatis, Emmanouil Glynos, Efstratios Stratikos, Dimitris Vlassopoulos, Henrich Frielinghaus, and Hermis Iatrou\*

Dimitrios Skoulas – Department of Chemistry, National and Kapodistrian University of Athens, 15771 Athens, Greece

Gaetano Mangiapia – German Engineering Material Science (GEMS) at Heinz Maier-Leibnitz Zentrum (MLZ), Helmholtz-Zentrum Hereon, 85748 Garching, Germany

Daniele Parisi – FORTH, Institute for Electronic Structure and Laser, 71110 Heraklion, Greece; Department of Materials Science & Technology, University of Crete, 71003 Heraklion, Greece

Maria Kasimatis – Department of Chemistry, National and Kapodistrian University of Athens, 15771 Athens, Greece

Emmanouil Glynos – FORTH, Institute for Electronic Structure and Laser, 71110 Heraklion, Greece; Department of Materials Science & Technology, University of Crete, 71003 Heraklion, Greece; [orcid.org/0000-0002-0623-8402](https://orcid.org/0000-0002-0623-8402)

Efstratios Stratikos – Department of Chemistry, National and Kapodistrian University of Athens, 15771 Athens, Greece

Dimitris Vlassopoulos – FORTH, Institute for Electronic Structure and Laser, 71110 Heraklion, Greece; Department of Materials Science & Technology, University of Crete, 71003 Heraklion, Greece; [orcid.org/0000-0003-0866-1930](https://orcid.org/0000-0003-0866-1930)

Henrich Frielinghaus – Jülich Centre for Neutron Science. JCNS at Heinz Maier-Leibnitz Zentrum (MLZ), Forschungszentrum Jülich GmbH, 85748 Garching, Germany; [orcid.org/0000-0002-8812-8783](https://orcid.org/0000-0002-8812-8783)

Hermis Iatrou – Department of Chemistry, National and Kapodistrian University of Athens, 15771 Athens, Greece; [orcid.org/0000-0001-9358-0769](https://orcid.org/0000-0001-9358-0769); Email: [iatrou@chem.uoa.gr](mailto:iatrou@chem.uoa.gr), Corresponding Author

---

**ABSTRACT:** Hydrogels that can respond to a number of external stimuli and at the same time show impressive rheological properties are promising materials for a wide range of bioapplications. Here, we present a series of well-defined linear amphiphilic pentablock hybrid polypeptides of the ABCBA type, where A is poly(L-lysine), B is poly(L-histidine)-*co*-poly( $\gamma$ -benzyl-L-glutamate), and C is poly(ethylene oxide) (PEO). The polymers were synthesized by the sequential primary amine ring-opening polymerization of *N*-carboxy anhydrides using bis amine poly(ethylene oxide) (PEO) as a bifunctional macroinitiator, and the length of all of the blocks was varied. The resulting materials formed novel extrudable in situ forming quickly self-healing hydrogels, responsive to the alteration of pH and increase of temperature. The connection between the alteration of the secondary structure of the polypeptides with the viscoelastic behavior was revealed by means of rheology and circular dichroism. Small-angle neutron scattering and scanning electron microscopy were employed to shed light on the structure of the polymers and how it affects their rheological properties. The obtained polymers were subjected to enzymatic degradation tests with trypsin and leucine aminopeptidase. The results suggest that these biomaterials have the potential to be used in a number of bioapplications like drug delivery, 3D printing, and tissue engineering.

---

## Introduction

The ever-increasing demands for synthetic materials that can be utilized in diagnostic and therapeutic applications have triggered the development of new biomaterials with novel properties that can replace damaged tissues<sup>1</sup> or can be used as carriers for drugs, proteins, or deoxyribonucleic acid (DNA) load.<sup>2,3</sup> Polymeric hydrogels are among the biomaterials that can be employed for biological applications since they can be highly responsive, functional, and versatile.<sup>4–7</sup> Depending on the polymeric material precursor that forms hydrogels, these materials can be biocompatible, can present a large variety of physical or chemical structures comprising their networks, and thus it is possible to tune their viscoelastic properties, which is very crucial for their

responsiveness. Therefore, hydrogels enjoy a prime position at the forefront of scientific research.<sup>8</sup>

Based on their molecular characteristics, hydrogels can be classified into several categories, such as natural and synthetic, chemically, or physically cross-linked as well as stimuli-responsive.<sup>9,10</sup> Among them, those hydrogels that originate from polypeptides present a combination of traits that offer a plethora of benefits. They can adopt secondary structure motifs that guide their self-assembly, leading to tunable rheological properties.<sup>11</sup> Their conformational structure can be modified depending on the environment, making them stimuli-responsive.<sup>12</sup> Additionally, they can present low cytotoxicity and sensitivity to biodegradation by enzymes, which render them appropriate for a number of bioapplications.<sup>13</sup>

Herein, linear pentablock hybrid quarter-polypeptides were synthesized, using the ring-opening polymerization (ROP) of *N*-carboxy anhydrides (NCAs).<sup>14,15</sup> Pentablock architecture ABABA, with hydrophobic B and hydrophilic A blocks, is known to yield hydrogels with higher gel moduli compared to the corresponding diblock and triblock polypeptides of AB and ABA types, due to better organized intrachain folding.<sup>16,17</sup> Gandhi and Maher<sup>18</sup> reported the enhanced elasticity of hydrogels from pentablock copolymers compared to those from triblock copolymers with similar molecular weights of two copolymers and different sizes of the blocks, due to the different assembly of the former.

In the last decades, research on the biological applications of polymeric materials has led many authors to suggest the covalent attachment of poly(ethylene oxide) (PEO) with polypeptides for the formation of hydrogels.<sup>19,20</sup> Brzezinska et al.<sup>21</sup> synthesized pentablock copolymers based on poly( $\gamma$ -benzyl-L-glutamate) (PBLG) with polyoctenamer, PEO, or poly(dimethylsiloxane) as the middle block and PEO as the outer blocks. Iijima et al.<sup>22</sup> used  $\alpha,\omega$ -diamino PEO as a macroinitiator in the middle block combined with ROP of NCAs for the synthesis of pentablock copolypeptides, which formed polymeric aggregates and hydrogels. PEO has also been utilized in an effort to produce thermoresponsive biomaterials. Huang et al. synthesized block copolymers containing a PEO block and an oligo(tyrosine) block, which exhibited thermoresponsive gelation.<sup>23</sup> The use of PEO to synthesize block copolymers with alanine or/and phenyl-alanine has been reported by the group of Jeong, who produced thermoreversible hydrogels.<sup>24,25</sup> Many researchers have used polypeptides, with monomeric units bearing short oligoethylene glycol (OEG) side chains,<sup>26,27</sup> which exhibit sol-gel transition and are therefore appropriate for in situ gel formation.<sup>28</sup>

The majority of the thermally responsive hydrogels presented thus far in the literature takes advantage of the increase in temperature, and/or pH, in the case of cancer treatment, when injected in the body to undergo a sol-gel transition and form the hydrogel. However, there is a lack of hydrogel systems in the literature that can actually respond to thermal stimuli and change their rheological properties to become weaker with increasing temperature, while simultaneously demonstrating multiple responsiveness to other stimuli like pH, enzymatic digestion, as well as exhibiting self-healing properties. In previous work,<sup>17</sup> we reported a noncytotoxic, in situ forming, injectable hydrogel that exhibits shear-thinning and rapid self-healing properties, based on fully polypeptide pentablock copolymer poly(L-lysine)-*b*-poly(L-histidine-*co*- $\gamma$ -benzyl-L-glutamate)-*b*-poly(L-lysine)-*b*-poly(L-histidine-*co*- $\gamma$ -benzyl-L-glutamate)-*b*-poly(L-lysine). The hydrogel was formed by physical interactions, providing buffering capacity, pH-responsive properties, as well as enzymatic biodegradation. In our effort to improve its responsiveness and further lower its toxicity, we envisioned a hydrogel that will additionally respond to temperature, while maintaining all of the functionalities already mentioned. For that purpose, we substituted the middle hydrophilic block of the polypeptides by PEO to generate a new family of hydrogels, with potentially more versatile properties. By altering the dimensions of the blocks, we studied their influence on the properties of the hydrogels in our effort to elucidate the structure-property relation.

In this work, we present a series of amphiphilic pentablock hybrid polypeptides of the type poly(L-lysine)-*b*-poly(L-histidine-*co*- $\gamma$ -benzyl-L-glutamate)-*b*-PEO-*b*-poly(L-histidine-*co*- $\gamma$ -benzyl-L-glutamate)-*b*-poly(L-lysine) (PLys-*b*-(PHis-*co*-PBLG)-*b*-PEO-*b*-(PHis-*co*-PBLG)-*b*-PLys) that can form extrudable (18G needle) in situ forming hydrogels. We present below the synthesized materials and their structural and

dynamic properties along with a thorough assessment. Our study can contribute to the design of tunable hydrogel materials that could serve several bioapplications. It was found that by altering the molecular dimensions of the different blocks, it was possible to fine-tune several properties such as strength of the hydrogel, time required for self-healing, as well as thermal and pH responsiveness. Therefore, depending on the application, it is possible to design a hybrid material to exhibit the required properties. The details of the various experimental techniques and protocols used are presented in the Supporting Information.

## Results and Discussion

**Synthesis of the Polymers.** All synthesized pentablock polypeptides of the ABCBA type are composed of one middle hydrophilic block (C = PEO) and two inner hydrophobic blocks (B = PHis-*co*-PBLG), flanked by two hydrophilic blocks of PLys (A), each one connected at the outer side of the middle hydrophobic block. The difunctional macroinitiator  $\alpha,\omega$ -bis(amine) PEO was used to initiate the ROP of the NCAs (Scheme 1). Furthermore, poly(L-histidine) (PHis) was selected due to its amphoteric nature within the physiological pH range, rendering the hydrogel pH-responsive.<sup>29</sup> The utilization of the trityl protecting group (Trt) to PHis monomeric units is the best way to avoid its racemization during deprotection.<sup>30</sup>

The goal was to investigate how the variation of the molecular weights of the middle PEO block, the hydrophobic blocks, and the outer hydrophilic PLys blocks can affect the viscoelastic properties of the hydrogels. Therefore, four series composed of eight different pentablock hybrid quarter-polypeptides were synthesized. On the first series, the molecular weight of PEO was varied, maintaining approximately the same molecular characteristics for the rest of the blocks, resulting polypeptides HG1, HG2, and HG3 (Table 1).

On the second series, the molecular weights of the two hydrophobic blocks PHis-*co*-PBLG were varied (Table 2). On the third series, we varied the outer PLys blocks, while we maintained the middle PEO block at  $2.0 \cdot 10^4$  g/mol and the hydrophobic blocks close to  $5.0 \cdot 10^4$  g/mol (Table 3). Finally, on the last series, the PLys blocks were varied keeping the PEO blocks at  $6.0 \cdot 10^3$  g/mol and the hydrophobic blocks close to  $5.0 \cdot 10^4$  g/mol (Table 4).

Based on our previous works,<sup>17</sup> we maintained the same ratio of the monomeric units of histidine and  $\gamma$ -benzyl-L-glutamate (50:50) in the hydrophobic blocks for all polymers since it was found that, at this ratio, the hydrogels remain pH-responsive and exhibit better rheological properties.

The combination of high-vacuum techniques and ROP, using a primary amine bifunctional initiator, yields polypeptides with narrow distribution of molecular weights, as demonstrated by size exclusion chromatography (SEC) eluograms. In addition, it offers the possibility to control the order of monomer addition, ensuring the hydrophilicity/hydrophobicity of each added block. The high purity of the synthesized NCAs is very critical for the living nature of the polymerization.<sup>15,30</sup> The molecular weights of the polypeptides obtained were within 10% of the molecular weights expected from the stoichiometry, i.e., the ratio of the monomeric units and the moles of the initiator. The complete monomer consumption as well as the successful deprotection of the monomeric units of histidine and lysine were confirmed by FT-IR spectroscopy (Figure S11, see the SI).

The protecting group of histidine moieties can be easily removed under mild conditions<sup>31</sup> without causing racemization. Also, the dialysis procedure is crucial for the pH neutralization and purification of the final polymer (presented in previous work).<sup>30</sup> The molecular weight of each block matched the monomer/macroinitiator ratios, which

confirm the good control over the molecular characteristics of the synthesized polypeptides. Upon completion of the polymerization of each block (confirmed by FT-IR spectra, Figure S11, see the SI), SEC characterization was performed. The SEC eluograms of the synthesis of pentablock terpolypeptide PLys-*b*-(PHis-co-PBLG)-*b*-PEO-*b*-(PHis-co-PBLG)-*b*-PLys (HG4) prior to deprotection are depicted in Figure S12 (see the SI). After deprotection, an SEC eluogram in water was not possible, not even in DMF, as the polypeptides formed hydrogels in water, while they did not dissolve at all in DMF. Furthermore, no nuclear magnetic resonance (NMR) spectrum was obtained because the final pentablock polypeptide was not soluble in common deuterated solvents.

**Hydrogel Formation.** The stiffness and strength of these hydrogels can be regulated by varying pH/temperature and also by altering their composition via the synthetic route. Indeed, by altering even one molecular characteristic, it is possible to obtain hydrogels with very different properties. It was found that the pentablocks should be well defined with a high degree of molecular and compositional homogeneity, otherwise no hydrogel formation was possible.

The formation of hydrogels using the synthesized materials is rather straightforward. The hybrid polypeptides PLys-*b*-(PHis-co-PBLG)-*b*-PEO-*b*-(PHis-co-PBLG)-*b*-PLys were weighed and placed into a vial, followed by the addition of Milli-Q water at a polymer/water ratio of 1:20. All synthesized polypeptides formed hydrogels, except HG8. Based on visual observation in the vial and quantitative characterization discussed below, HG5 formed a weak hydrogel, which was turned into liquid after gentle shaking, while HG7 formed an even weaker hydrogel. All hydrogels were formed immediately, except HG6 and HG7, which needed some time (approximately 20 min). HG1 and HG2 hybrid polypeptides formed very strong hydrogels compared to the softer and brittle hydrogel of our previous work<sup>17</sup> or other hydrogels of this study. They maintained their gel texture even after shaking, as indicated by the way HG1 was attached to tweezers (TOC figure). For these hydrogels, further addition of Milli-Q water did not cause dilution (which could not be excluded a priori since they are physical), but rather saturation. HG4 was the most promising hydrogel based on its viscoelastic behavior since it formed a strong extrudable hydrogel that was extruded even from a thin needle 18G.

**Circular Dichroism.** Circular dichroism measurements were performed to elucidate the secondary structure of the polypeptides, which significantly influences their organization and thus their rheological properties. All samples were diluted to low concentrations ( $5 \cdot 10^{-4}$  g/mL). It should be mentioned that the very strong hydrogels (HG1 and HG2) could not be diluted under any dilution. Therefore, we performed the measurements only for samples HG3-HG7, which had a PEO connector of  $2.0 \cdot 10^4$  g/mol and different polypeptide molecular characteristics. PEO does not contribute to circular dichroism.

The circular dichroism spectra of the synthesized polymers are shown in Figure 1. A negative peak at 197 nm is present in all samples except HG6 (shorter poly(L-lysine) block than hydrophobic block), which is characteristic of the random coil conformation and correlates to poly(L-lysine) (see SI Figure S10). All polypeptides exhibit a negative peak at 225–230 nm<sup>-1</sup>. The existence of this peak is attributed to the  $\alpha$ -helices of PBLG. We presented in our previous work that the presence of  $\alpha$ -helices is critical for the ability of the pentablocks to form a strong hydrogel.<sup>17</sup> By performing a subtraction of the poly(L-lysine) random coil conformation spectrum from the overall spectrum of HG4, a spectrum of  $\alpha$ -helix was obtained similar to the one of our previous publication (Figure 2C in ref 17). In that particular publication, we proved that

the participation of the PBLG in the hydrophobic blocks plays a pivotal role, as it promotes the formation of a secondary structure that stabilizes the 3D polypeptide network. Since the molecular characteristics of the PHis-co-PBLG part were exactly the same in this work,  $\alpha$ -helix is formed, which governs the formation of the hydrogel.

**Enzymatic Degradation.** Hydrogels of the type PLys-*b*-(PHis-co-PBLG)-*b*-PEO-*b*-(PHis-co-PBLG)-*b*-PLys can be biodegraded by enzymes due to their polypeptide nature. Furthermore, these hydrogels may not need to be removed from the body after the release of their cargo in any potential drug delivery application. There are numerous enzymes that can biodegrade these hydrogels. Among them, leucine aminopeptidase (LAP), an exopeptidase that catalyzes the hydrolysis of amino acid residues from the amino terminus of polypeptide chains, and trypsin, an endopeptidase that can cleave the amide bond of lysine residues from its C-terminus, are of great interest. Trypsin is expressed in different types of human cancer cell lines like colorectal, gastric, breast, lung, stomach, and pancreatic cancer cell lines, and it is involved in the malignant growth of tumor cell,<sup>32–35</sup> while LAP is an abundant cytosolic metabolic enzyme that may be released to the medium when the cell is lysed.

HG4 was chosen to be tested against both enzymes due to its superior rheological properties (see below) as well as pH and temperature responsiveness (see Figure 2). A sample was removed at specific time lapses and reacted with fluorescamine.<sup>36</sup> The product of this reaction was used to calculate the rate of enzymatic degradation of the hydrogel via fluorescence (Table 5). L-Lysine, which is the product of biodegradation, was utilized for the preparation of PBS solutions at different concentrations to react with fluorescamine under the same conditions as the biodegraded HG4 samples and was used as a standard for the quantification of enzyme degradation (see SI Figures S13 and S14). It was found that the hydrogel was degraded by both enzymes, although much faster by trypsin. In addition, the specific activity of both enzymes for this type of hydrogels was larger compared to the one obtained in our previous work for hydrogels of the type PLys-*b*-(PHis-co-PBLG)-PLys-*b*-(PHis-co-PBLG)-*b*-PLys.<sup>17</sup> This can be attributed to the easier accessibility of the monomeric units and the terminal amino group of polypeptides by enzymes, in comparison to the hydrogels presented in our previous work. Probably PEO remains at the interior of the aggregates rendering the polypeptides more susceptible to the bulky enzymes.

**Scanning Electron Microscopy (SEM).** Hydrogel samples were rapidly frozen with liquid nitrogen, and they were then lyophilized under high vacuum prior to SEM analysis. For all samples, it was noticed that the polypeptide block contributes to the characteristic 3D organization with the formation of cavities, while PEO is probably mixed with the polypeptidic fibril mesh. PEO is distinguished in the SEM images because it forms small structures (with the appearance of 2D flat surfaces) or spherical aggregates, while the polypeptide blocks form long fibrillar 3D network structures (see Figure 3). This can be seen in our previous publication of the SEM of hydrogels formed by fully polypeptidic materials.<sup>17</sup> The strongest network formed by HG1, which is the polymer with the smallest PEO connector and the smallest outer blocks, has the smallest dimensions of fibrils and cavities alike.

As the length of the PEO increases, the characteristic structural length increases, as well as 2D structures are formed by the crystalline PEO moieties as in the case of HG3, which has the same polypeptide blocks but approximately triple amount of PEO compared to HG1. The SEM images give the impression of porous material, and as we move from HG1 to HG2 and HG3, we observe a more heterogeneous network with a larger apparent pore size.

Comparing HG3 and HG7, it seems that by increasing the outer block of poly(L-lysine), the size of the cavities and the length of the fibrils increase further. This is attributed to the larger amount of the polypeptide block, which probably forms long 3D fibrils. We note that HG7 is liquid in appearance. HG6 exhibits a weaker structure with a larger average size of weakly anisotropic pores (or cavities) and thinner "walls" between cavities compared to HG3. Therefore, larger dimensions of the cavities combined with thinner fibrils are directly linked to the weakening of the hydrogel's strength of HG6, making it more easily deformable and difficult to flow.

Further support for this comes from the rheology and SANS results discussed below. Actually, HG6 has a larger hydrophobic block than HG3 and forms elongated domains in aqueous solutions (see Table 6). HG4 comprises the appropriate ratio of hydrophobic to hydrophilic blocks for the formation of a strong and stable hydrogel, and as a result, a 3D structure with cavities in close distances was formed, as seen for pH = 7.4 (Figure 3). However, the HG4 hydrogel at pH 5 yielded a dissolved network without a 3D structure, i.e., without cavities and fibrils. At lower pH values, due to the protonation of histidine, PHis becomes hydrophilic and its 3D structure is collapsed. HG5 could barely form a hydrogel, in agreement with rheology data discussed below; hence, it was not analyzed by SEM. The homogeneity of the 3D network is an indication of the successful synthesis and the low-molecular-weight distribution, which influences the rheological properties. It was revealed that by altering the length of any block of the polymer during the synthetic process, modification of its self-organization is possible, yielding hydrogels with different viscoelastic properties.

**Rheology.** The rheological properties of the hydrogels were investigated with the aim to study the responsiveness of the hydrogels to alteration of pH and temperature. Besides responsiveness, the investigated hydrogels exhibited yielding upon application of nonlinear shear, rapid, and complete reversibility (self-healing) after flow cessation, which makes them extrudable (see relevant discussion below). HG4, which encompasses all of the above-mentioned attributes, can be easily extruded through an 18G (1.2 × 38 mm<sup>2</sup>) needle and does not collapse after extrusion. It responds to alteration of temperature, especially between 25 and 37 °C as well as between 37 and 41 °C.

All samples were investigated at a concentration of 5% (w/w) in water (ratio w/w polymer/water = 1:20). A saturation point was observed at that concentration for HG1 and HG2, as the excess water remained unabsorbed from the hydrogel. HG5 and HG7 formed very weak hydrogels. In particular, HG7 exhibited liquid-like properties and was excluded from further rheological investigations. Before discussing the rheological data and relevant figures below, a note is in order. Given the very limited amount of samples available, the measurements were performed with small geometries (see the SI) and the scattering of the viscoelastic signal (confirmed by the values of moduli) was unavoidable. The reported data are reproducible. Where possible (in terms of amount), repeat experiments were performed with two different loadings, yielding same results within an error of 8% (error bars within the symbols in all figures). Hence, despite the noise, the message emerging from the data, as described below, is clear and unambiguous.

The dynamic strain amplitude sweep data (Figure S17, see the SI) indicate that all hydrogels have a very narrow linear viscoelastic regime (of strain-independent moduli) at the frequency of 1 rad/s and a low yield strain (assigned at the  $G' - G''$  crossover, marking the transition from the low-strain solid-like to the high-strain liquid-like regime) ranging from about 0.2% (HG5) to about 42% (HG2). HG4 exhibited a more extended linear viscoelastic regime and a larger yield strain of

about 10% (the respective shear rate at 1 rad/s is 0.1 s<sup>-1</sup>). The yield properties indicate the ability to handle the hydrogels, in particular to make them flow through a syringe and maintain their coherence thereafter via fast self-healing (discussed below). The associated yield stress is about 20 Pa. This value makes the particular HG4 hydrogel suitable for injectable needle administration of type 18G.

Next, we present the linear viscoelastic spectra of the hydrogels in terms of their distinct molecular characteristics (see also Tables 1–4): (i) constant polypeptide PHis-co-PBLG mass and varying PEO mass (Figure 4, left) and (ii) the opposite, constant PEO mass and varying PHis-co-PBLG mass.

We observe that the shortest length of PEO yields the strongest hydrogel. Indeed, HG1 with a PEO molecular weight of 5.95 × 10<sup>3</sup> g/mol has the larger value of the plateau modulus  $G'$  of about 3 kPa, throughout the entire frequency range examined, despite the scattering of the data (Figure 4). We wish to emphasize here that while the same specific protocol was applied to all samples and tried to ensure steady conditions (see SI), at the molecular level, there are processes that may take longer time and may yield a slight increase in  $G'$  at low frequencies, which is evident for HG1 with a lower fraction of PEO (Figure 4, left). However, given that the sample was sealed with PDMS, evaporation was excluded; hence, the small changes in moduli should reflect the equilibration process of the hydrogel. On the other hand, HG3 with larger effective porosity and heterogeneity (Figure 3) exhibits lower plateau modulus at high frequencies (about 1.5 kPa) and a tendency to flow (though the low-frequency response is characterized by an apparent self-similar decrease of the moduli with an approximate power-law exponent of about 0.5). This picture is consistent with the SANS analysis presented below.

To examine the role of the polypeptide blocks on the rheological behavior of the hydrogels, we synthesized polypeptides with the same PEO length (corresponding to 20.0 × 10<sup>3</sup> g/mol) while altering the number of the monomeric units of the amino acids (samples HG3, HG4, HG5, HG6, and HG7). HG4 has a double number of monomeric units of lysine in comparison to HG3, while the rest of the molecular characteristics remain the same.

The hydrogel HG4 exhibited linear viscoelastic properties characterized by large and extended plateau modulus (Figure 4) and large deformability as inferred by the yield strain (Figure S17). Comparison of the properties of HG4 with those of HG5 and HG6 suggests that altering the composition of the hydrophobic polypeptide block (with respect to HG4) by increasing (HG6) or decreasing (HG5) the number of monomeric units of PHis-co-PBLG leads to weaker hydrogels.

For HG5, the high-frequency plateau  $G'$  drops by a factor of about 2 with respect to HG4, but importantly, the material shows a clear tendency toward a terminal crossover to flow at about 0.4 rad/s (unfortunately, we faced an issue with the instrument software, while measuring the HG5 sample and we could only recover the limited data reported in Figure 4, right). On the other hand, for HG6, the modulus drops by about one decade without evidence of terminal response. This may be naively rationalized by a crude, qualitative correlation between the average length scale extracted from the modulus and the structural size scale from TEM. The images in Figure 5 indicate an increase of the average cavity size  $\xi$  from HG4 to HG6 by a factor of about 5 (Figure 3). If such a size is considered to be a reasonable representation of the average mesh size of the bulk hydrogel, it yields an apparent modulus value of  $kT/\xi^3$ , which respectively increases by one decade. As mentioned, this is nothing more than an interesting correlation, but the rheological data

are also consistent with the formation of elongated effective aggregates formed by the hydrophobic groups, as revealed by the SANS analysis (Table 6 and Figure 9). Although more work will be needed to extract an unambiguous quantitative picture, these findings point to the importance of the synthetic process, and in particular the delicate role of the molecular composition of the pentablocks in the properties of the resulting hydrogels.

Next, we discuss the temperature and pH dependence of the viscoelastic properties of HG4 (Figures 5 and 6). Although an increase in temperature from 25 to 41 °C has a mild impact on the high-frequency regime, or small length scales, the low-frequency region (0.01–0.1 rad/s) is remarkably affected, with the material response prone to change from viscoelastic solid to viscoelastic liquid. Specifically, this can be observed when the loss factor ( $\tan(\delta) = G''/G'$ ) approaches unity (Figure 5) and, equivalently, the low-frequency response is characterized by self-similar moduli (i.e., parallel with respect to frequency) with a power-law exponent of about 0.2 (Figure 6). In fact, this only happens at a pH value of 6.5. When the pH is 7.4, a change in temperature has no noticeable effect on the rheological properties of HG4 (Figure S16, SI). This can be explained as follows: PEO is temperature-sensitive,<sup>37</sup> since at higher temperatures, it dehydrates and becomes hydrophobic. At pH = 7.4, the strength of hydrogel depends mainly on the fibrils of the polypeptide blocks, which are not affected by the temperature. At lower pH values, the polypeptide fibril network is loose or even collapsed, and thus, the responsiveness of PEO to temperature affects the rheological properties of the hydrogel (Figure 6). At higher temperatures, PEO aggregates, the organization of the fibrils weakens further, and eventually the hydrogel collapses (see also Table 7). Hence, HG4 displays pH dependence and thermo-responsiveness at the same time. The distinct viscoelastic behavior between 37 and 41 °C (Figure 5) renders this specific system highly suitable for drug delivery applications, and particularly for applications aiming at cancer treatment due to the narrow window of temperature responsiveness.

The effect of pH on the linear viscoelastic response at 37 °C is much more evident than the thermal effect at constant pH. As the pH varies from 6.5 to 7.4 the elasticity of the system increases by almost 1 order of magnitude (see  $\tan(\delta)$  in Figure 5, right). The reason lies on the fact that the change of the secondary structure of the polypeptide blocks, due to the alteration of pH, makes the hydrogel stronger at pH = 7.4, where we have a combination of the  $\beta$ -turn conformation of PHis and  $\alpha$ -helices of PGLG. HG1 also exhibits temperature responsiveness between 25 and 37 °C, without a change of pH (SI, Figure S15). For this hydrogel, due to its smaller molecular dimensions (Figure 3), dehydration of PEO is much stronger at the same temperature, affecting the rheological properties substantially.

Figure 7 demonstrates the self-healing ability of hydrogel HG4 at  $T = 37$  °C. In particular, it shows two sequential dynamic time sweep (DTS) tests at a frequency of 1 rad/s and different strain amplitudes: (i)  $\gamma_0 = 200\%$  in the strongly nonlinear regime, where the gel yields (breaks) immediately (at about 0.2 s), a test often called rejuvenation with eventually constant moduli and  $G'' > G'$  (over a duration of 300 s here). (ii)  $\gamma_0 = 0.1\%$  in the linear regime, to assess the reversibility of the viscoelastic properties, i.e., recover of the solid-like behavior ( $G' > G''$ ) of the hydrogel, which is a measure of the so-called self-healing. We observe here that although the exact original values of the moduli are recovered at about 5 s, subsequently, they drop and remain smaller than the original values at the onset of the first test (by about a factor of 2 for  $G'$  and a factor of 6 for  $G''$ ) after about 50 s, while always  $G' > G''$ .

We attribute this to the possible effect of tool inertia when switching the strain amplitude from 200 to 0.1% and the possibility that the sample was expelled from the geometry during the large-amplitude oscillatory shearing (something that could be not readily checked with the sealing fluid and covered geometry), as well as the possibly different organization of this metastable hydrogel. Nevertheless, we would like to emphasize that the nonideal experiment provides convincing evidence of the self-healing ability of the (abruptly) yielded HG4 hydrogel, which instantly transforms into a viscoelastic solid immediately upon cessation of the imposed large-amplitude oscillatory shear.

*Small-Angle Neutron Scattering.* Scattering cross sections are reported in Figures 8 and 9. In the first plot (Figure 8), data for hydrogels HG1, HG2, HG3, HG4, HG6, and HG7 at pH = 7.4 measured at 37 °C are shown (HG5 and HG8, which do not form or form very weak gels, were not investigated). For HG4, which has been proved to show the highest linear rheological regime, a temperature scan from 37 to 60 °C was carried out, with the pH kept constant at 6.5: in this case, the cross sections are displayed in Figure 9.

Inspection of the plots reveals that it is possible to distinguish two main Q regions in the trend of the cross sections:

- (i) A region at a medium–high Q ( $Q > 7 \cdot 10^{-3} \text{ \AA}^{-1}$ ), where a “shoulder” is present. This signal arises from the scattering of the hydrophobic domains of the hydrogels that are organized into micelles or micellar aggregates. In this case, due to the molecular structure, hydrophilic PEO chains act either as a bridge connecting two “adjacent” aggregates or folds on the same aggregate (the so-called “loop”), depending on the physicochemical conditions, such as concentration, temperature, pH, etc. This Q region represents the “boundary” under which the Guinier regime of the aggregates is observed. On the other hand, going toward high Q values, the scattering signal decreases by some decades and the incoherent contribution coming from the hydrogel molecular composition, as well as from the solvent, becomes relevant.
- (ii) A region at a low Q ( $Q < 7 \cdot 10^{-3} \text{ \AA}^{-1}$ ), where the scattering cross section scales with a power law, i.e.,  $d\Sigma/d\Omega \propto Q^{-p}$ , showing the fractal behavior of the gel network at this length scale. High intensities suggest high internal stresses in the hydrogel.

The trend qualitatively described is typical of the hydrogels,<sup>38</sup> where a hierarchical organization occurs, consisting of several characteristic length scales, although the Q range embraced in the present case by the SANS measurements may give an overview of the structure only over a length scale between  $\cong 10 \text{ \AA}$  and 0.3  $\mu\text{m}$ , anyway well below the resolution limit of the SEM images ( $\sim 100 \text{ nm}$ ). In this regard, the micellar aggregates may be considered as “primary particles”, which represent, in turn, the basic units forming the gel network at larger length scales, whose appearance is well visible from SEM images (Figure 4). The gel organization can be thus suitably described through the concept of fractal, decomposing the total cross section in the sum of the scattering arising from the different length scales.

For these kinds of structures, the unified model developed by Beaucage is very appropriate to extract structural parameters of the hierarchical arrangement of the gel.<sup>39</sup> In this approach, each structural level is described by a Guinier power law and an associated power law regime. Theoretical cross sections for an  $n$ -level structure may be described as

$$\frac{d\Sigma}{d\Omega} = \sum_{i=1}^n \left\{ G_i \exp\left(-\frac{Q^2 R_{gi}^2}{3}\right) + B_i \left[ \operatorname{erf}^3\left(\frac{QR_{gi}}{\sqrt{6}}\right) \frac{1}{Q} \right]^{p_i} \right\} + \left(\frac{d\Sigma}{d\Omega}\right)_{\text{incoh}} \quad (1)$$

where  $R_{gi} (< R_{gi+1})$  represents the radius of gyration of the  $i$ -th structure level contributing to the total cross section and  $p_i$  is the exponent with which the cross sections scale, according to the fractal dimension. Finally,  $(d\Sigma/d\Omega)_{\text{incoh}}$  is the incoherent contribution to the scattering cross section. In eq 1, it is assumed that the levels are separated in  $Q$ , with no overlap between two different levels, a condition which is most of the time fulfilled.

In the  $Q$  range of the systems under investigation, since  $n = 2$  and taking into account that the Guinier regime for the upper level falls in the ultra-SANS (USANS) domain, we have  $Q \cdot R_{g2} \gg 1$ , so the equation may be simplified as

$$\frac{d\Sigma}{d\Omega} = B_2 Q^{-p_2} + G_1 \exp\left(-\frac{Q^2 R_{g1}^2}{3}\right) + B_1 \left[ \operatorname{erf}^3\left(\frac{QR_{g1}}{\sqrt{6}}\right) \frac{1}{Q} \right]^{p_1} + \left(\frac{d\Sigma}{d\Omega}\right)_{\text{incoh}} \quad (2)$$

Equation 2 corresponds to the application of Beaucage's formalisms to our system, which, in a general manner, may be expressed by eq 1. According to this formalism, in a system having a hierarchical arrangement, like that of a gel, each structural level is described by a Guinier term and a power law term. The first term represents the scattering behavior in the region where  $Q$  (the modulus of the scattering vector) is comparable to or smaller than the inverse of the gyration radius  $R_{gi}$  of the scattering structure, whereas the second term describes the cross sections in the region where  $Q \cdot R_{gi} > 1$ , where cross sections scale with a power law whose exponent is  $p$ . The terms  $G$  and  $B$  represent the proportionality factors having a dependence on the volume fraction of the gel.

Equation 2 was fitted to the experimental cross sections to get structural information through the analysis of extracted parameters, which are reported in Tables 6 and 7. It is interesting to start the analysis with systems measured at a constant temperature (37 °C, Figure 8). Here, the most noticeable feature is the position of the shoulder at intermediate  $Q$  values, which shows consistent variations: the highest values are observed for systems HG1 and HG2, whereas for the other hydrogels, there is a comparable shifting at lower  $Q$  values. The second prominent feature is represented by the power laws observed in the intermediate- and low- $Q$  regions, as indicated by dashed lines in Figure 8. Given the expected structural organization of the hydrogel, it is reasonable to assume that the primary particles as spheroidal or elongated particles having a rough surface and thus behaving as a surface fractal, whose scattering cross section scales as  $(d\Sigma/d\Omega) \propto Q^{-(6-d_s)}$ ,<sup>40</sup> where  $d_s$  is the surface fractal dimension,<sup>40</sup> which is connected to the slope  $p_1$ . In turn, the gel network at larger distances, formed by "clusters" of primary particles, is expected to be a mass fractal, whose dimension  $d_m$  gives the compactness of the network and coincides with the exponent  $p_2$  of the power law found in the low- $Q$  region  $(d\Sigma/d\Omega) \propto Q^{-d_m}$ ,<sup>40</sup>

*Linking Structure and Dynamics.* We now attempt to combine the results from SANS, SEM, and rheology to assess the investigated hydrogels in a consistent way. The above analysis of the results may be rationalized in terms of the molecular structure: this latter ultimately influences the aggregate architecture, which is responsible for the gel properties. To facilitate the analysis, it is profitable to discuss in detail the systems where one parameter at a time has changed. Thus, a comparison between the systems HG1, HG2, and HG3 may reveal the effect of increasing the length of the PEO chains along with the results in Figures 3 and 4. On the other hand, a comparison between HG3 and HG6 gels may provide insights into the effect of increasing the length of the hydrophobic block PHis-co-PBLG. Finally, the comparison of the systems HG3, HG4, and HG7 is important to elucidate the effect of the length of the Lys chains. However, before discussing the experimental results, it should be

emphasized that the comparisons have to be nevertheless managed carefully since other parameters, such as temperature and pH, may strongly affect the gel properties and, inevitably, here, we chose to examine only a certain range.

Analysis of gels HG1, HG2, and HG3 reveals that an increase in PEO chain length increases the size of the primary aggregates, whose gyration radius displays a tendency to larger values. While from HG1 to HG2 the step is not observable due to the overweight of the two outer blocks, in the last step to HG3, a change is clearly visible. This is an expected behavior because of the increase of the molecular size, in agreement with the enhanced apparent porosity (Figure 3) and approach to terminal relaxation (Figure 4) of HG3. This characteristic is also clear from the  $Q$  shifting of the position of the shoulder in Figure 8. The results listed in Table 6 show that the length of PEO does not affect sensibly the compactness of the hydrogels at large length scales since the fractal dimension of the network is comparable for all three systems. More interesting is the decrease of the scattering due to the gel network, which is visible at a low  $Q$ . Here, to show in a better way the cross sections of all of the systems, data have been multiplied for different scale factors. Taking into account such factors, it is apparent that the cross-section values decrease going from HG1 to HG3, if compared at the same (low)  $Q$  value. This is even more apparent for HG3 as well as easily detectable by a direct comparison of the  $B_2$  pre-factor listed in Table 6. In fact, the concentration of the block copolymer is constant for all of the systems and if larger particles are formed at the nanoscopic level, these particles are more "diluted" at larger length scales, which means that the network will be expected to appear "looser" with better self-healing properties. This result is supported by the rheology results discussed above (Figure 4), which indicate that HG1 gel is the strongest hydrogel compared to HG2 and HG3 (with HG4, they are the strongest gels investigated). A tighter gel network as observed in terms of rheology, as for HG1, although with smaller primary aggregates in terms of radius of gyration, could influence the arrangement at the micrometer length scale as observed in terms of the SEM images. Indeed, the comparison of SEM images in Figure 3 suggests that from HG1 to HG3, the dimension (effective cavity size) of the network increases.

The comparison between HG3 and HG6 systems may allow getting insights into the effect of the hydrophobic block PHis-co-PBLG on the gel structure: for HG6, the length of this block is doubled, but inspection of Table 6 shows that this results only in a slight increase of the aggregate size, from  $\cong 100$  to  $\cong 105$  Å, anyway well above the statistical uncertainty affecting the data. Because of a larger hydrophobic part, we speculate that the gel HG6 has primary aggregates with a higher aggregation number of PHis-co-PBLG molecules, even if a very small increase in  $R_{g1}$  suggests that possibly the shape of such particles in HG6 is somehow elongated, rather than spheroidal. This finding suits our expectations due to the large extent of PEO chains that in many cases promote, through interchain repulsion,<sup>41</sup> the formation of aggregates with a larger packing factor, leading to the formation of cylindrical or worm-like micelles in HG6. The ability to relax internal stresses is diminished.

We now discuss the effects of increasing the length of the external PLYs chain, as done in HG3, HG4, and HG7 (where the number of repetitive units goes from 60 and 120 up to 180 units) in conjunction with the SEM results of Figure 3. The size of the primary aggregates is within the experimental uncertainty for HG3 and HG4 gels,  $\cong (100 \pm 1)$  Å, reducing up to 93 Å. An increase in the hydrophilic/hydrophobic balance could reduce the driving force of the aggregate formation and possibly also the shape of the primary particles. Actually, the circular dichroism measurements have shown a different behavior for HG7 in comparison to HG3 and HG4. The peak at  $\cong 200$  nm in Figure 1 should be

progressively more intense as soon as the relative number of Lys increases: HG7 shows indeed a lower and quite flat signal, which could suggest a different conformation of the PLys chains, due to their large length. Furthermore, the formation of the gel network has different characteristics, as shown by the unusual slope with which the cross sections scale in the low-Q region. A possible influence of these findings is found at the micrometer (large) length scale, where HG7 exhibits the largest cavities (Figure 3) supporting its liquid-like appearance.

The presence of long chains of PLys, each repeating unit of which carries a free amino group capable of being protonated at acidic pH, has suggested studying the hydrogel behavior at lower pH values and at different temperatures, to have insights into the resistance of the structure. Thus, HG4 has been studied at pH 6.5 and at temperatures in the range of 37–60 °C (see also Figures 5 and S16). Inspection of Figure 9 suggests that the trend of scattering cross sections is similar to those observed for the other gels and that the higher is the temperature, the less pronounced is the scattering from primary particles. This is also evident from the analysis of the parameters in Table 7. Although the dimension of the primary aggregates slightly increases with temperature, going from  $\cong 96$  to 104 Å, the scattering contribution of such structures decreases drastically when the temperature increases. It is well known<sup>42</sup> that increasing the temperature makes the PEO blocks more hydrophobic promoting in parallel the expulsion of hydration water. This leads to higher aggregation numbers (thus to higher dimensions of the aggregate), but, because of this behavior, to primary aggregates which have on average a higher correlation distance, being more “diluted” in the gel network, and making it weaker but increased relaxation abilities for internal stresses. This agrees again with the rheology results (Figure 5), showing that for the sample HG4 at pH 6.5, the gel becomes weaker with the increase of temperature, as well as the SEM results (Figure 3), showing a change in porosity. It has also to be noted that a change in pH could provide significant changes in the particle shapes: in particular, the formation of more curved aggregates should be expected, although this cannot be evidenced from the analysis of the cross-sectional trend in the high-concentration regime used to prepare gel systems.<sup>43</sup>

### Conclusions

A series of well-defined amphiphilic linear pentablock hybrid polypeptides of the ABCBA type were synthesized using precise chemistry, where A is PLys, C is PEO, and B is PHis-co-PBLG block. The chain lengths of the blocks were varied, to obtain hydrogels with different viscoelastic properties. The synthesis of the polymers yielded a novel extrudable in situ forming and very quickly self-healing hydrogel with responsiveness to triple stimuli, namely, pH, temperature, and enzymes. Interestingly, it was found that the temperature responsiveness occurs only under lower-pH conditions. This is very critical for the directional and targeted delivery of cargo from the hydrogel toward cancer tissues in drug delivery applications since these tissues have lower pHs and higher temperatures. These characteristics render the hydrogel appropriate for a wide gamut of bioapplications, such as drug delivery, 3D printing (self-healing property), and tissue engineering. It was revealed that any change in the composition of the polymers can affect the rheological and structural properties of these hydrogels. The secondary structure of the polypeptide blocks plays a critical role in the rheological behavior of the hydrogel. The combination of precise chemistry with multifunctional materials leads to unique responsive versatile hydrogels, which can be used as a possible platform to facilitate advanced biomedical applications. Our present systematic comparative investigation revealed that hydrogel HG4 is the optimum for the specific drug delivery application: under the same conditions of pH and temperature, it possesses a high-plateau modulus to

ensure coherence, as well as large yield strain and fast recovery, allowing easy handling, for exchange during the injection process. These features are similar to those of HG1, which however is less sensitive to temperature in the range of 37–41 °C at the same pH, due to the main difference of these two hydrogels and the total molar fraction of hydrophobic blocks (39 and 59% for HG1 and HG4, respectively, see Tables 1 and 3). Future work will investigate the possibility of incorporation of anticancer drugs into these hydrogels and further utilization as drug delivery systems.

### Associated Content

Supporting Information contains the following:

Sample preparation, size exclusion chromatography, NMR spectroscopy, circular dichroism, rheology, fluorescence measurements, SEM, small-angle neutron scattering, SEC eluograms, FT-IR spectra, and dynamic frequency sweep rheology measurements (PDF)

### Notes

The authors declare no competing financial interest.

### Acknowledgments

The Maier-Leibnitz Center (MLZ) is fully acknowledged for the scientific support and for provision of beam time. The present work was funded by the European Union and Greek national funds through the Operational Program “Competitiveness, Entrepreneurship and Innovation”, under the call “RESEARCH-CREATE-INNOVATE” (project code: T1EAK-01612).

### REFERENCES

- (1) Prabhakaran, M. P.; Venugopal, J.; Kai, D.; Ramakrishna, S. Biomimetic material strategies for cardiac tissue engineering. *Mater. Sci. Eng., C* 2011, 31, 503–513.
- (2) Langer, R.; Peppas, N. A. Advances in biomaterials, drug delivery, and bionanotechnology. *AIChE J.* 2003, 49, 2990–3006.
- (3) Segura, T.; Chung, P. H.; Shea, L. D. DNA delivery from hyaluronic acid-collagen hydrogels via a substrate-mediated approach. *Biomaterials* 2005, 26, 1575–1584.
- (4) Kopecek, J. Hydrogel biomaterials: A smart future? *Biomaterials* 2007, 28, 5185–5192.
- (5) Drury, J. L.; Mooney, D. J. Hydrogels for tissue engineering: scaffold design variables and applications. *Biomaterials* 2003, 24, 4337–4351.
- (6) Hoare, T. R.; Kohane, D. S. Hydrogels in drug delivery: Progress and challenges. *Polymer* 2008, 49, 1993–2007.
- (7) Peppas, N. A.; Huang, Y.; Torres-Lugo, M.; Ward, J. H.; Zhang, J. Physicochemical, foundations and structural design of hydrogels in medicine and biology. *Annu. Rev. Biomed. Eng.* 2000, 2, 9–29.
- (8) Kopecek, J. Hydrogels: From Soft Contact Lenses and Implants to Self-Assembled Nanomaterials. *J. Polym. Sci., Part A: Polym. Chem.* 2009, 47, 5929–5946.
- (9) Ullah, F.; Othman, M. B. H.; Javed, F.; Ahmad, Z.; Akil, H. M. Classification, processing and application of hydrogels: A review. *Mater. Sci. Eng., C* 2015, 57, 414–433.
- (10) Liarou, E.; Varlas, S.; Skoulas, D.; Tsimblouli, C.; Sereti, E.; Dimas, K.; Iatrou, H. Smart polymersomes and hydrogels from polypeptide-based polymer systems through  $\alpha$ -amino acid N-carboxyanhydride ring-opening polymerization. From chemistry to biomedical applications. *Prog. Polym. Sci.* 2018, 83, 28–78.
- (11) Shen, Y.; Fu, X. H.; Fu, W. X.; Li, Z. B. Biodegradable stimuli-responsive polypeptide materials prepared by ring opening polymerization. *Chem. Soc. Rev.* 2015, 44, 612–622.
- (12) Tian, B.; Tao, X. G.; Ren, T. Y.; Weng, Y.; Lin, X.; Zhang, Y.; Tang, X. Polypeptide-based vesicles: formation, properties and

- application for drug delivery. *J. Mater. Chem.* 2012, 22, 17404–17414.
- (13) Chandrawati, R. Enzyme-responsive polymer hydrogels for therapeutic delivery. *Exp. Biol. Med.* 2016, 241, 972–979.
- (14) Deming, T. J. Synthesis and Self-Assembly of Well-Defined Block Copolypeptides via Controlled NCA Polymerization. In *Hierarchical Macromolecular Structures: 60 Years after the Staudinger Nobel Prize II*; Percec, V., Ed.; Springer International Publishing, 2013; Vol. 262, pp 1–37.
- (15) Hadjichristidis, N.; Iatrou, H.; Pitsikalis, M.; Sakellariou, G. Synthesis of Well-Defined Polypeptide-Based Materials via the Ring-Opening Polymerization of  $\alpha$ -Amino Acid N-Carboxyanhydrides. *Chem. Rev.* 2009, 109, 5528–5578.
- (16) Li, Z. B.; Deming, T. J. Tunable hydrogel morphology via selfassembly of amphiphilic pentablock copolypeptides. *Soft Matter* 2010, 6, 2546–2551.
- (17) Bilalis, P.; Skoulas, D.; Karatzas, A.; Marakis, J.; Stamogiannos, A.; Tsimblouli, C.; Sereti, E.; Stratikos, E.; Dimas, K.; Vlassopoulos, D.; Iatrou, H. Self-Healing pH- and Enzyme Stimuli-Responsive Hydrogels for Targeted Delivery of Gemcitabine to Treat Pancreatic Cancer. *Biomacromolecules* 2018, 19, 3840–3852.
- (18) Gandhi, J. V.; Maher, J. V.; Shaffer, K. A.; Chapman, T. M. Capillary wave studies of multiblock polypeptide copolymers at the air/water interface. *Langmuir* 1997, 13, 5933–5940.
- (19) Veronese, F. M.; Pasut, G. PEGylation, successful approach to drug delivery. *Drug Discovery Today* 2005, 10, 1451–1458.
- (20) Hamidi, M.; Azadi, A.; Rafiei, P. Pharmacokinetic consequences of pegylation. *Drug Delivery* 2006, 13, 399–409.
- (21) Brzezinska, K. R.; Curtin, S. A.; Deming, T. J. Polypeptide endcapping using functionalized isocyanates: Preparation of pentablock copolymers. *Macromolecules* 2002, 35, 2970–2976.
- (22) Iijima, M.; Ulkoski, D.; Sakuma, S.; Matsukuma, D.; Nishiyama, N.; Otsuka, H.; Scholz, C. Synthesis of PEGylated poly(amino acid) pentablock copolymers and their self-assembly. *Polym. Int.* 2016, 65, 1132–1141.
- (23) Huang, J.; Hastings, C. L.; Duffy, G. P.; Kelly, H. M.; Raeburn, J.; Adams, D. J.; Heise, A. Supramolecular Hydrogels with Reverse Thermal Gelation Properties from (Oligo)tyrosine Containing Block Copolymers. *Biomacromolecules* 2013, 14, 200–206.
- (24) Choi, Y. Y.; Joo, M. K.; Sohn, Y. S.; Jeong, B. Significance of secondary structure in nanostructure formation and thermosensitivity of polypeptide block copolymers. *Soft Matter* 2008, 4, 2383–2387.
- (25) Kang, E. Y.; Yeon, B.; Moon, H. J.; Jeong, B. PEG-L-PAF and PEG-D-PAF: Comparative Study on Thermogelation and Biodegradation. *Macromolecules* 2012, 45, 2007–2013.
- (26) Gharakhanian, E. G.; Deming, T. J. Role of Side-Chain Molecular Features in Tuning Lower Critical Solution Temperatures (LCSTs) of Oligoethylene Glycol Modified Polypeptides. *J. Phys. Chem. B* 2016, 120, 6096–6101.
- (27) Chen, C. Y.; Wang, Z. H.; Li, Z. B. Thermoresponsive Polypeptides from Pegylated Poly-L-glutamates. *Biomacromolecules* 2011, 12, 2859–2863.
- (28) Lu, D. D.; Wang, H. S.; Li, T. E.; Li, Y. F.; Wang, X. Y.; Niu, P. F.; Guo, H. Y.; Sun, S. B.; Wang, X. Q.; Guan, X. L.; Ma, H. C.; Lei, Z. Q. Versatile Surgical Adhesive and Hemostatic Materials: Synthesis, Properties, and Application of Thermoresponsive Polypeptides. *Chem. Mater.* 2017, 29, 5493–5503.
- (29) Patchornik, A.; Berger, A.; Katchalski, E. Poly-L-histidine. *J. Am. Chem. Soc.* 1957, 79, 5227–5230.
- (30) Mavrogiorgis, D.; Bilalis, P.; Karatzas, A.; Skoulas, D.; Fotinogiannopoulou, G.; Iatrou, H. Controlled polymerization of histidine and synthesis of well-defined stimuli responsive polymers. Elucidation of the structure-aggregation relationship of this highly multifunctional material. *Polym. Chem.* 2014, 5, 6256–6278.
- (31) Sieber, P.; Riniker, B. Protection of Histidine in peptide synthesis - A reassessment of the trityl group. *Tetrahedron Lett.* 1987, 28, 6031–6034.
- (32) Soreide, K.; Janssen, E. A.; Korner, H.; Baak, J. P. A. Trypsin in colorectal cancer: molecular biological mechanisms of proliferation, invasion, and metastasis. *J. Pathol.* 2006, 209, 147–156.
- (33) Miyata, S.; Koshikawa, N.; Higashi, S.; Miyagi, Y.; Nagashima, Y.; Yanoma, S.; Kato, Y.; Yasumitsu, H.; Miyazaki, K. Expression of trypsin in human cancer cell lines and cancer tissues and its tight binding to soluble form of Alzheimer amyloid precursor protein in culture. *J. Biochem.* 1999, 125, 1067–1076.
- (34) Nakanuma, S.; Tajima, H.; Okamoto, K.; Hayashi, H.; Nakagawara, H.; Onishi, I.; Takamura, H.; Kitagawa, H.; Fushida, S.; Tani, T.; Fujimura, T.; Kayahara, M.; Ohta, T.; Wakayama, T.; Iseki, S.; Harada, S. I. Tumor-derived trypsin enhances proliferation of intrahepatic cholangiocarcinoma cells by activating protease-activated receptor-2. *Int. J. Oncol.* 2010, 36, 793–800.
- (35) Kato, Y.; Nagashima, Y.; Koshikawa, N.; Miyagi, Y.; Yasumitsu, H.; Miyazaki, K. Production of trypsin by human gastric cancer cells correlates with their malignant phenotype. *Eur. J. Cancer* 1998, 34, 1117–1123.
- (36) Bantan-Polak, T.; Kassai, M.; Grant, K. B. A comparison of fluorescamine and naphthalene-2,3-dicarboxaldehyde fluorogenic reagents for microplate-based detection of amino acids. *Anal. Biochem.* 2001, 297, 128–136.
- (37) Vanparijs, N.; Nuhn, L.; De Geest, B. G. Transiently thermoresponsive polymers and their applications in biomedicine. *Chem. Soc. Rev.* 2017, 46, 1193–1239.
- (38) Kanji, K. *Gels Handbook, The Fundamentals*; Elsevier, 2001; Vol. 1, pp 122–171.
- (39) Beaucage, G. Combined Small-Angle Scattering for Characterization of Hierarchically Structured Polymer Systems over Nano-to-Micron Meter: Part II Theory. In *Polymer Science: A Comprehensive Reference*, 10 Volume Set; Elsevier, 2012; Vol. 2, pp 399–409.
- (40) Brumberger, H. *Modern Aspects of Small-Angle Scattering*; Springer Netherlands, 1995; p XV463.
- (41) D'Errico, G.; Silipo, A.; Mangiapia, G.; Vitiello, G.; Radulescu, A.; Molinaro, A.; Lanzetta, R.; Paduano, L. Characterization of liposomes formed by lipopolysaccharides from *Burkholderia cenocepacia*, *Burkholderia multivorans* and *Agrobacterium tumefaciens*: From the molecular structure to the aggregate architecture. *Phys. Chem. Chem. Phys.* 2010, 12, 13574–13585.
- (42) Mitchell, D. J.; Tiddy, G. J. T.; Waring, L.; Bostock, T.; McDonald, M. P. Phase behaviour of polyoxyethylene surfactants with water. Mesophase structures and partial miscibility (cloud points). *J. Chem. Soc., Faraday Trans. 1* 1983, 79, 975–1000.
- (43) Hirama, T.; Lu, S. M.; Kay, J. G.; Maekawa, M.; Kozlov, M. M.; Grinstein, S.; Fairn, G. D. Membrane curvature induced by proximity of anionic phospholipids can initiate endocytosis. *Nat. Commun.* 2017, 8, No. 1393.

FIGURES

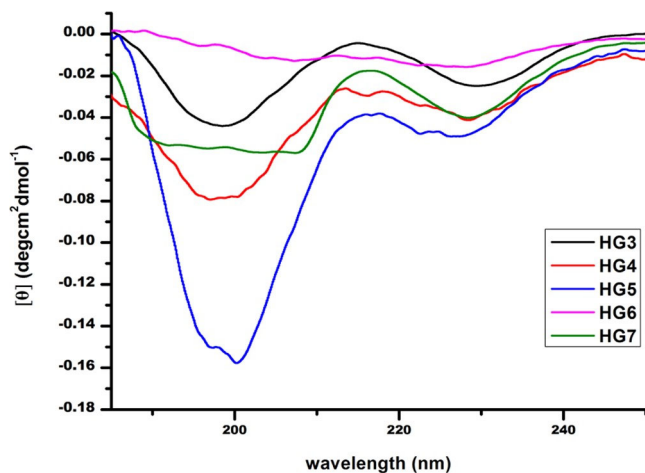


Figure 1. Circular dichroism spectra of the synthesized polymers.

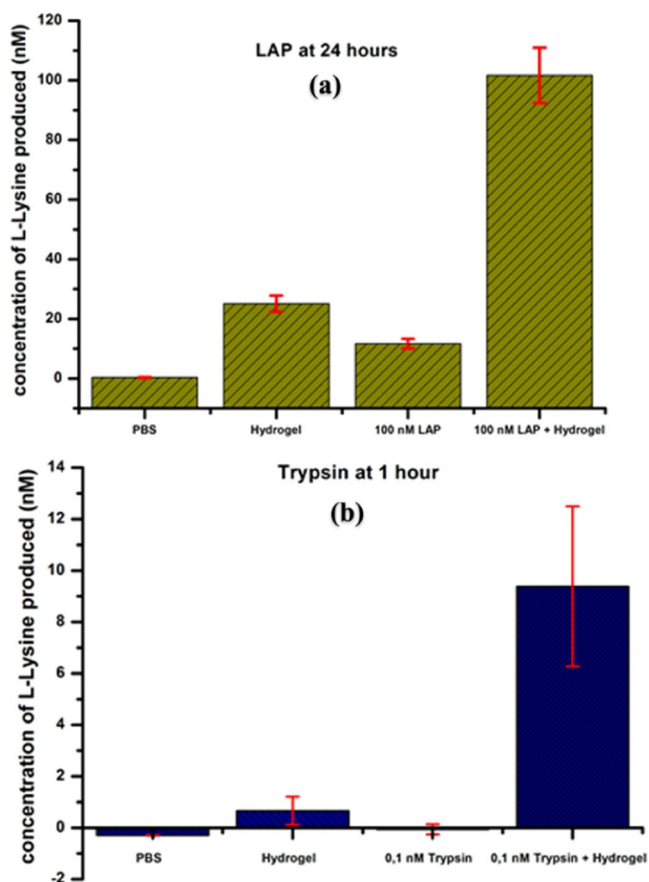


Figure 2. Biodegradation of hydrogel HG4 by (a) LAP at 24 h and (b) trypsin at 1 h of incubation at 37 °C.

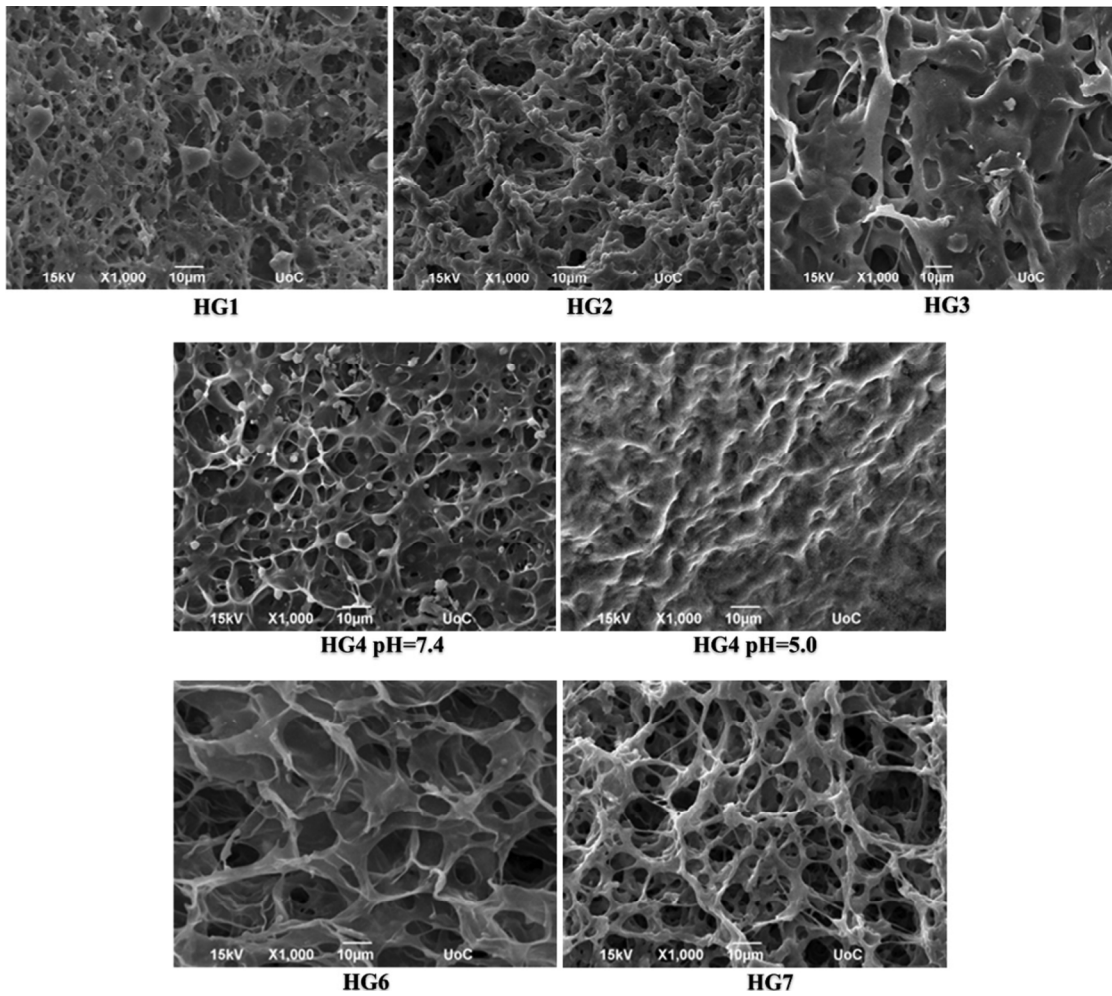


Figure 3. Scanning electron microscopy images of hydrogels at pH = 7.4 when the pH value is not mentioned

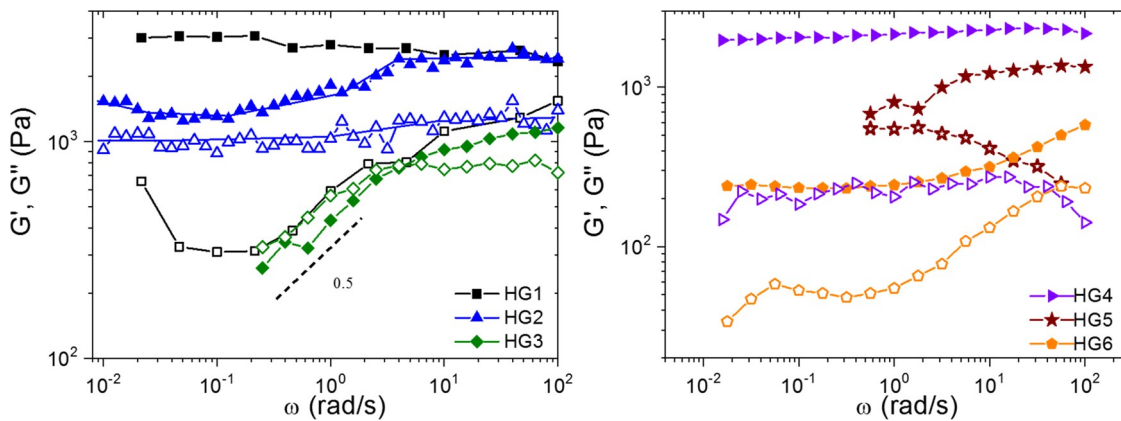


Figure 4. Frequency-dependent storage  $G'$  (solid symbols) and loss  $G''$  (open symbols) moduli for the hydrogels HG1, HG2, and HG3 (left) and HG4, HG5, and HG6 (right). Experiments were performed at  $T = 25\text{ }^{\circ}\text{C}$ ,  $\text{pH} = 7.4$ , and strain amplitude 0.5% for HG1 and HG6, and 0.1% for HG2, HG3, HG4, and HG5. Lines are a guide to the eye. The apparent slight increase of  $G'$  in HG1 with decreasing frequency reflects equilibration issues.

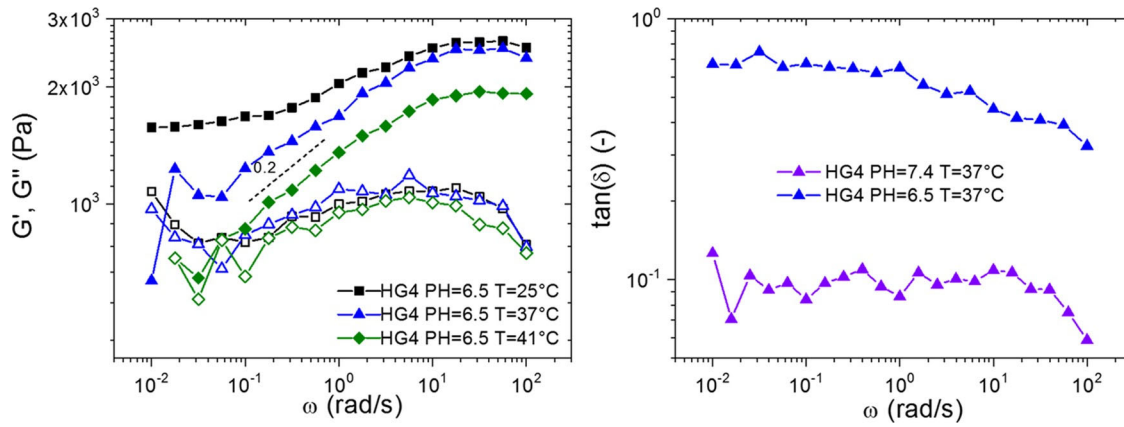


Figure 5. Left: Frequency-dependent storage  $G'$  (solid symbols) and loss  $G''$  (open symbols) moduli for the hydrogel HG4 at 25 °C (squares), 37 °C (triangles), and 41 °C (diamonds) at pH = 6.5. Right: loss factor  $\tan(\delta) = G''/G'$  at pH = 7.4 and 6.5 at 37 °C. The strain amplitude was 0.1% for all of the temperatures. The slope of 0.2 indicates the apparent power-law exponent at 37 and 41 °C. Lines are a guide to the eye

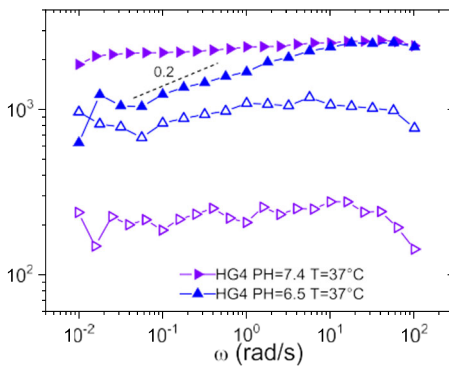


Figure 6. Frequency-dependent storage  $G'$  (solid symbols) and loss  $G''$  (open symbols) moduli for the hydrogel HG4 at 37 °C and pH = 7.4 (right-pointed triangles) and pH = 6.5 (top-pointed triangles). The strain amplitude was fixed to 0.1%. Lines are a guide to the eye.

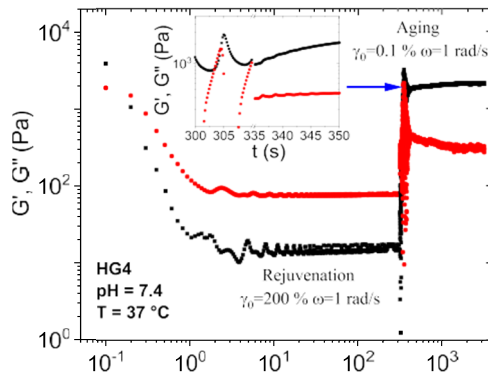


Figure 7. Experimental procedure to determine the self-healing ability of hydrogel HG4 at pH = 7.4 and  $T = 37$  °C. It involves two sequential tests: (i) Dynamic time sweep depicting the storage  $G'$  (black symbols) and loss  $G''$  (red symbols) moduli as a function of time at a strain amplitude of 200% and oscillatory frequency  $\omega = 1$  rad/s (strongly in the nonlinear regime) for a duration of 300 s, where the hydrogel yields a liquid at about 0.2 s and the moduli remain eventually constant with  $G'' > G'$ . (ii) Dynamic strain sweep follows immediately with a strain amplitude of 0.1% (within the linear viscoelastic regime),  $\omega = 1$  rad/s for 3000 s. It instantly leads to hydrogel reformation with  $G' > G''$ ; hence, it provides evidence of self-healing (see text for details).

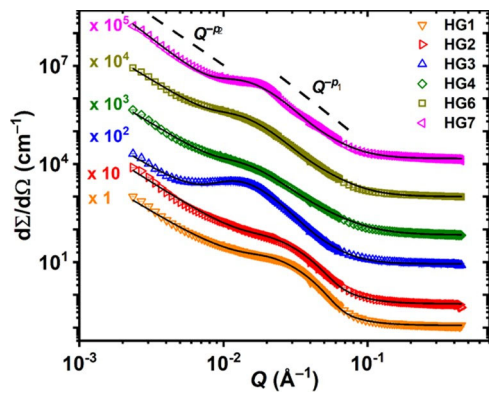


Figure 8. Scattering cross sections obtained at 37 °C for the samples reported in the legend. Gel HG4 has been measured at pH = 7.4. For a better visualization, data have been multiplied for a scale factor, as indicated. Black solid lines have been obtained through fitting of [eq 2](#) to the experimental data

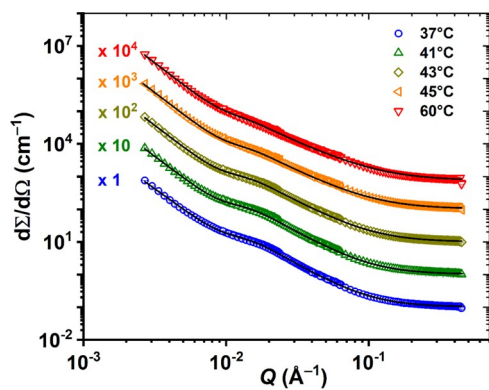
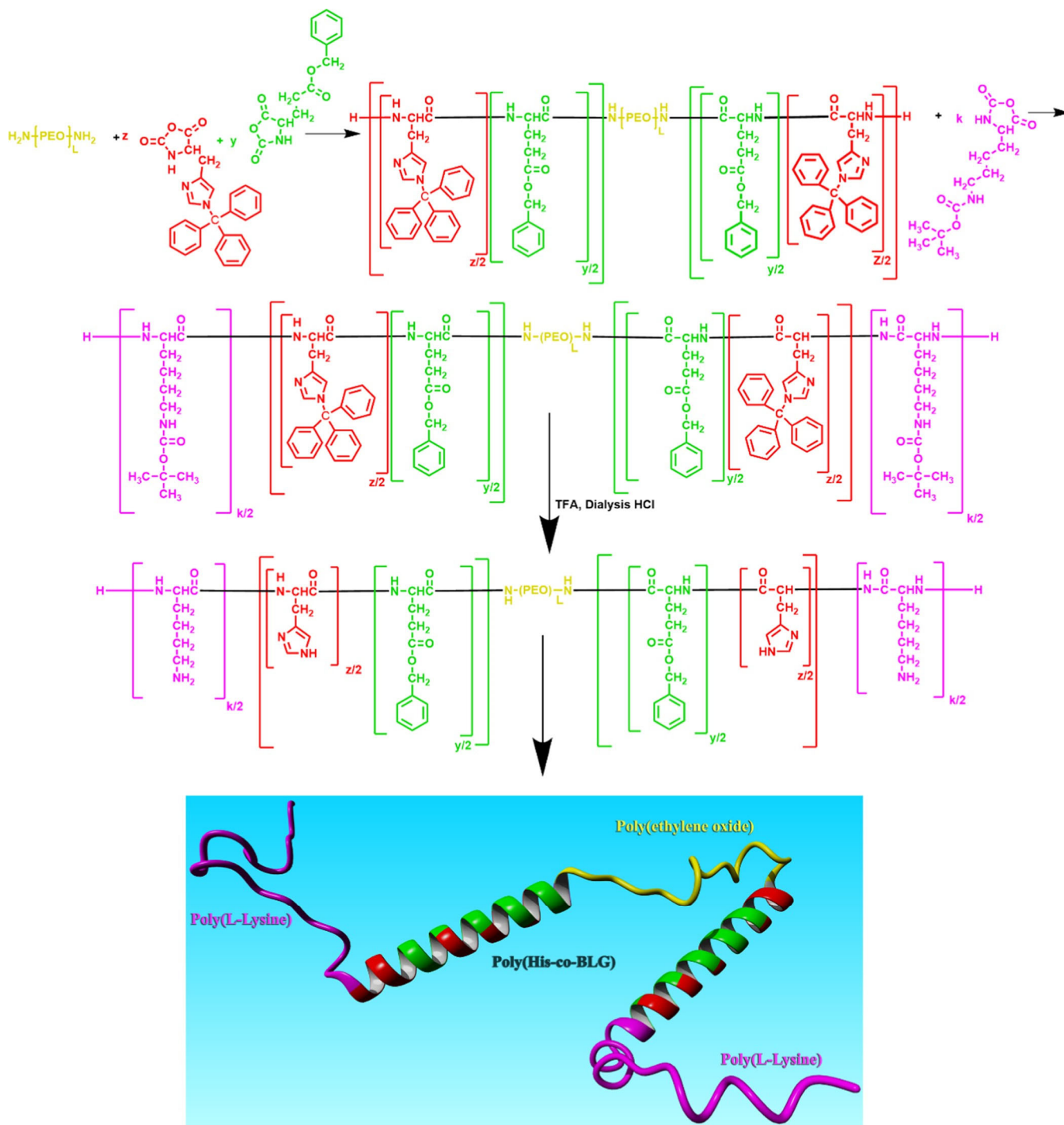


Figure 9. Scattering cross sections obtained for sample HG4 at pH = 6.5 and at several temperatures as reported in the legend. For a better visualization, data have been multiplied for a scale factor, as indicated. Black solid lines have been obtained through fitting of [eq 2](#) to the experimental data.

SCHEMES



Scheme 1. Synthetic Route for the Hybrid Polypeptides of the Type PLys-*b*-(PHis-co-PBLG)-PEO-*b*-(PHis-co-PBLG)-*b*-PLys

TABLES

Table 1. Molecular Characteristics of the Synthesized Polymers prior to Deprotection with Varying Middle PEO Block

Hydrogel/Sample	$M_n$ central block (PEO) · 10 <sup>-3</sup> (g/mol)*	$M_n$ triblock PHis-co-PBLG/PEO/total · 10 <sup>-3</sup> (g/mol)*	$M_n$ protected pentablock · 10 <sup>-3</sup> (g/mol)*	$M_n$ external PLys · 10 <sup>3</sup> protected (g/mol)	$D^*$
HG1	5.95	48.0/5.95/53.9	81.3	27.4	1.09
HG2	10.0	48.0/10.0/58.0	85.4	27.4	1.10
HG3	20.0	48.0/20.0/68.0	95.4	27.4	1.12

\* Obtained by SEC-TALLS in DMF with 0.1 N LiBr at 60 °C.

Table 2. Molecular Characteristics of the Synthesized Polymers prior to Deprotection with Varying Two Hydrophobic Blocks PHis-co-PBLG

Hydrogel/Sample	$M_n$ central block (PEO) · 10 <sup>-3</sup> (g/mol)*	$M_n$ triblock PHis-co-PBLG/PEO/total · 10 <sup>-3</sup> (g/mol)*	$M_n$ protected pentablock · 10 <sup>-3</sup> (g/mol)*	$M_n$ external PLys · 10 <sup>3</sup> protected (g/mol)	$D^*$
HG3	20.0	48.0/20.0/68.0	95.4	27.4	1.12
HG5	20.0	24.1/20.0/44.0	71.6	27.5	1.10
HG6	20.0	95.8/20.0/115.7	143.2	27.5	1.12

\* Obtained by SEC-TALLS in DMF with 0.1 N LiBr at 60 °C.

Table 3. Molecular Characteristics of the Synthesized Polymers prior to Deprotection with Varying Two Hydrophilic External Blocks Poly(L-lisine)

Hydrogel/Sample	$M_n$ central block (PEO) · 10 <sup>-3</sup> (g/mol)*	$M_n$ triblock PHis-co-PBLG/PEO/total · 10 <sup>-3</sup> (g/mol)*	$M_n$ protected pentablock · 10 <sup>-3</sup> (g/mol)*	$M_n$ external PLys · 10 <sup>3</sup> protected (g/mol)	$D^*$
HG3	20.0	48.0/20.0/68.0	95.4	27.4	1.12
HG4	20.0	47.9/20.0/67.8	122.6	54.8	1.13
HG7	20.0	48.0/20.0/68.0	150.1	82.1	1.14

\* Obtained by SEC-TALLS in DMF with 0.1 N LiBr at 60 °C.

Table 4. Molecular Characteristics of the Synthesized Polymers prior to Deprotection with Varying Two Hydrophobic Blocks PHis-co-PBLG

Hydrogel/Sample	$M_n$ central block (PEO) · 10 <sup>-3</sup> (g/mol)*	$M_n$ triblock PHis-co-PBLG/PEO/total · 10 <sup>-3</sup> (g/mol)*	$M_n$ protected pentablock · 10 <sup>-3</sup> (g/mol)*	$M_n$ external PLys · 10 <sup>3</sup> protected (g/mol)	$D^*$
HG1	5.95	48.0/5.95/53.9	81.3	27.4	1.09
HG8	5.95	48.0/5.95/53.9	136.1	82.1	1.15

\* Obtained by SEC-TALLS in DMF with 0.1 N LiBr at 60 °C.

Table 5. Specific activity of LAP and Trypsin for HG4

Sample	Specific activity LAP (s <sup>-1</sup> mg hydrogel <sup>-1</sup> )	Specific activity Trypsin (s <sup>-1</sup> mg hydrogel <sup>-1</sup> )
HG4	9.7x10 <sup>-6</sup> ± 4.12x10 <sup>-6</sup>	0.395 ± 2.1x10 <sup>-4</sup>

Table 6. Microstructural Parameters Obtained through the Fitting of Eq 2 to the Experimental Data. HG4 refers to the system at pH 7.4.

System	$\frac{10^5 \cdot B_2}{\text{cm}^{-1} \text{Å}^{p_2}}$	$p_2$	$\frac{10 \cdot B_1}{\text{cm}^{-1} \text{Å}^{p_1}}$	$\frac{G_1}{\text{cm}^{-1}}$	$\frac{R_{g_1}}{\text{Å}}$	$p_1$	$100 \cdot \frac{(d\Sigma/d\Omega)_{\text{incoh}}}{\text{cm}^{-1}}$
HG1	4.8±0.6	2.75±0.02	0.82±0.06	15.5±0.4	62.0±0.2	3.78±0.17	11.67±0.09
HG2	2.7±0.4	2.80±0.03	0.32±0.04	5.6±0.3	62.3±0.5	3.72±0.12	5.33±0.08
HG3	0.8±0.3	2.79±0.06	1.062±0.016	12.4±0.5	99.7±0.9	3.63±0.04	8.86±0.06
HG4	4.0±0.7	2.66±0.03	1.07±0.04	3.0±0.3	100.2±0.9	2.69±0.03	6.78±0.05
HG6	6.1±1.0	2.71±0.03	1.32±0.06	12.0±0.9	104.9±0.7	3.18±0.03	10.06±0.09
HG7	0.17±0.06	3.44±0.06	2.53±0.06	16.2±1.1	93.9±0.7	3.19±0.12	14.73±0.13

Table 7. Microstructural Parameters Obtained for the System HG4 at pH = 6.5 and at Different Temperatures through the Fitting of Eq 2 to the Experimental Data

$\frac{T}{^\circ\text{C}}$	$\frac{10^6 \cdot B_2}{\text{cm}^{-1} \text{Å}^{p_2}}$	$p_2$	$\frac{B_1}{\text{cm}^{-1} \text{Å}^{p_1}}$	$\frac{G_1}{\text{cm}^{-1}}$	$\frac{R_{g_1}}{\text{Å}}$	$p_1$	$100 \cdot \frac{(d\Sigma/d\Omega)_{\text{incoh}}}{\text{cm}^{-1}}$
37	6.0±0.7	3.14±0.02	0.280±0.003	1.0±0.4	95.9±0.8	2.31±0.02	10.33±0.07
41	2.8±0.4	3.26±0.02	0.291±0.003	0	98.0±0.8	2.29±0.02	10.32±0.08
43	2.0±0.2	3.305±0.019	0.285±0.003	0	98.2±0.8	2.172±0.010	10.11±0.06
45	1.7±0.2	3.33±0.02	0.282±0.003	0	97.4±1.5	1.985±0.012	10.30±0.07
60	1.30±0.19	3.35±0.02	0.234±0.003	0	104±2	1.854±0.015	7.63±0.09